Supplementary Information

Supporting Information S1: Optimization of B_0 Field for fatScalp and metBrain Shim for the ACDC Shim Array

A. fatScalp ACDC shim

For the optimization procedure to find the optimal fatScalp, we considered the inversion pulse as a band-stop filter with five regions, an inversion band, two bands without inversion, and two transition bands. Since it is usually impossible to have all the lipids fully in the inversion band, while having the metabolites fully inside of the no-inversion band, we minimized the number of metabolite voxels incidentally inverted, in addition to minimizing the number of lipid voxels left uninverted. Minimizing the number of violated voxels, or the ℓ_0 pseudo norm of the vector of violations is not tractable and thus we solve a simplified problem: We minimize the ℓ_1-norm of the violation, the convex envelope of the ℓ_0-ball as described mathematically and graphically below

$$\min_{x,f_c,s_b,s_k,m_{sk}} \alpha\|s_b\|_1 + (1-\alpha)\|s_{sk}\|_1$$

$$A_b x + b_b + s_b \geqslant f_c + \frac{\Delta f_{tb}}{2}$$

$$A_{sk} x + b_{sk} - s_{sk} \leqslant f_c - \frac{\Delta f_{tb}}{2}$$

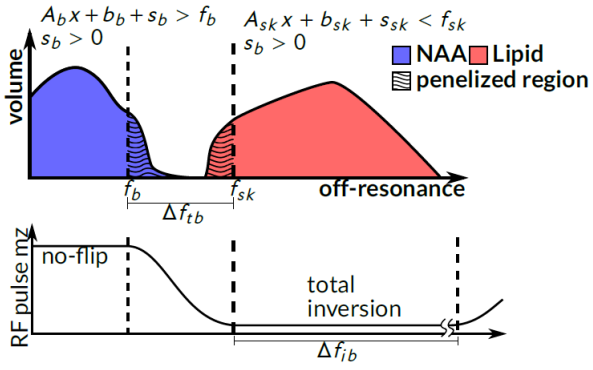

where the subscripts b and sk represent the corresponding variable within the brain or skull, respectively; α is the weight to either emphasize minimizing uninverted skull

voxels, or inverted brain voxels; s are slack variables to allow some of the skull voxels to be not or only partially inverted, and some of the brain voxels to be inverted; A is the shim basis; x is the vector of currents driven through each shim-loop; b_m and b_{sk} are the NAA and lipid frequencies in the brain and the skull, respectively; f_c is the center frequency of the inversion band; Δf_{tb} is the frequency range of the transition band (the one between NAA and lipids) of the inversion pulse.**Supporting Information S2: Lipid suppression of the 2.24 ppm lipid peak**

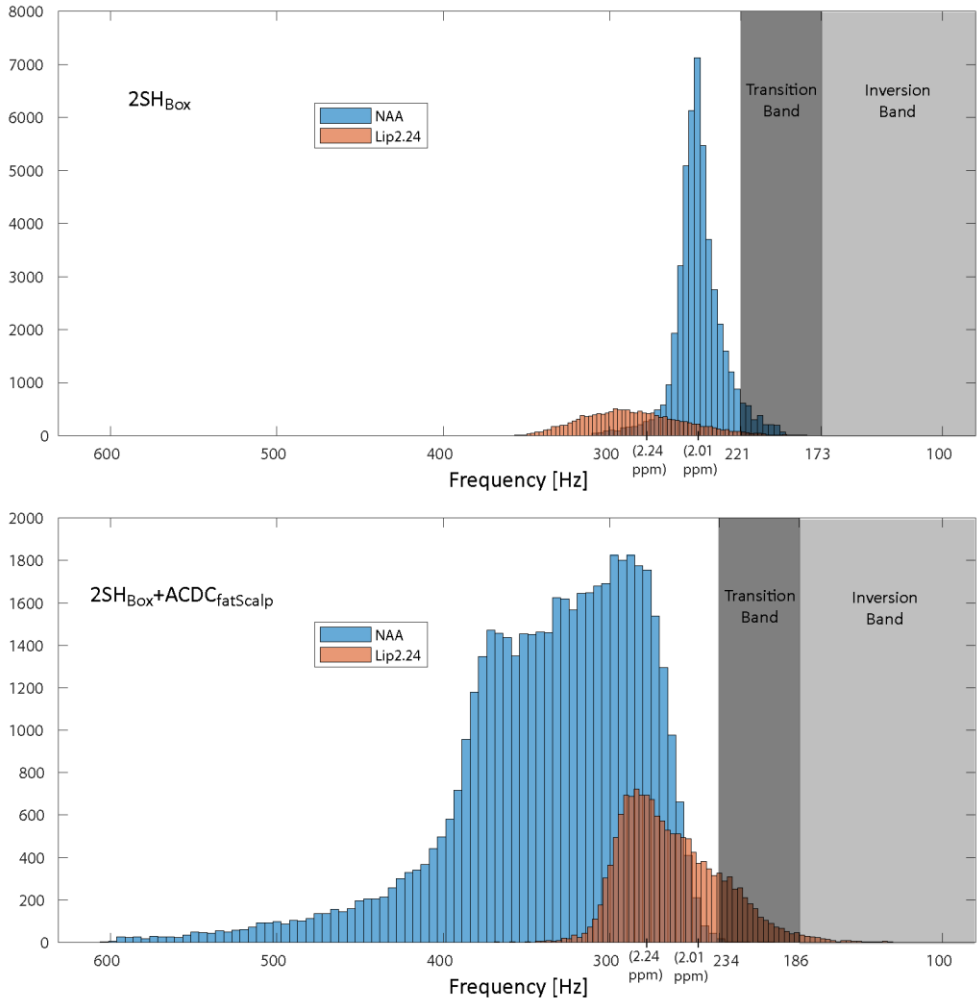

Supporting Information Figure SF1. Suppression of the lipid peak at 2.24 ppm investigated in one volunteer: a) The upper panel shows the 2SH$_{Box}$ histograms of the NAA peak at 2.01 ppm in the brain compartment and the lipid peak at 2.24 ppm within the lipid layer; b) the lower panel shows the 2SH$_{Box}$+ACDC$_{fatScalp}$ histograms of the NAA peak at 2.01 ppm and a lipid peak at 2.24 ppm. The transition band of the HGSB pulse is shown as the dark grey shaded area, with the inversion band to its right in light grey. The 2SH$_{Box}$+ACDC$_{fatScalp}$ can help to partially suppress other lipid peaks in addition to the 1.3 ppm and 0.9 ppm peaks. For example, the 2SH$_{Box}$+ACDC$_{fatScalp}$ can move the 2.24 ppm lipid peak into the transition or even inversion band

of the HGSB lipid inversion pulse, where they are partially or fully inverted, and thus will be reduced. For this volunteer, the percentages of lipid signals inside the transition or inversion bands are 100 %, 99 %, 51 %, 33 %, and 1 % for the lipid peaks at 1.3 ppm, 1.59 ppm, 2.02 ppm, 2.24 ppm, and 2.77 ppm, respectively. All other lipid peaks are fully in the no-inversion band.

B. metBrain ACDC shim

Following fatScalp, the shim array can be reconfigured for metBrain to minimize the inhomogeneity in the brain within the slab of interest. After brain masking the shim basis and baseline inhomogeneity to include only the brain-in-slab volume, we compute shim currents by minimizing the ℓ_2-norm of the off-resonance in the brain. Linear constraints limit individual current per channel to 2A, and the total current to 25 A for the entire array. The minimization formulation is given below:

$$\text{minimize}_x \ \|A_b x + b_b\|_2^2$$

$$\text{subject to: } \|x\|_1 \leq I_{tot} \ \wedge \ |x_i| \leq I_{max}$$

Supporting Information S3: Pulse Details

The BIR-4 adiabatic pulse had a duration of 8 ms, 1 kHz bandwidth and 23 μT maximum B1 amplitude, and 78° Ernst flip angle. The BIR-4 pulse consisted of four adiabatic half passage (AHP) HS-16 pulses with a 5 kHz adiabatic sweep. Two gradient modulated adiabatic refocusing GOIA-W (16,4) pulses (34) of 5 ms and 20 kHz bandwidths were used with a maximum B_1 amplitude of 17 μT (140 % above the adiabatic threshold). For lipid suppression, a frequency-selective adiabatic inversion was performed with a hypergeometric single band (HGSB) pulse of 44 ms with numerical parameters A=4.58, B=0.26, C=-6.5, D=9.5 and Ω=12.24 (35), which provided

an inversion bandwidth of 2 kHz and a narrow transition band of 48 Hz. The maximum B_1 field for the HGSB pulse was set at 17 μT (150 % above the adiabatic threshold). The asymmetry factor of our HGSB pulse is 0.935 and the inversion happens in the last 3 ms of the pulse. Hence, the inversion recovery times vary only by 3 ms for different offset frequencies. Off-resonance frequencies therefore have a negligible effect on the inversion time.

Supporting Information S4: Basis Set Simulations

The basis set for LCModel fitting was simulated in GAMMA with the same pulse modulations played on the scanner and included the following metabolites: D-2-hydroxyglutarate, Alanine, Ascorbate, Aspartate, Creatine, Ethanolamine, γ-Aminobutyric acid, Glycerophosphocholine, Glycerophosphoethanolamine, Glutathione, Glucose, Glutamine, Glutamate, Glycine, myo-Inositol, Lactate, N-acetylaspartylglutamate, NAA, Phosphocholine, Phosphocreatine, Phosphorylethanolamine, scyllo-Inositol, Serine, Taurine, Threonine. No lipids or macromolecules were included in the basis sets.

Supporting Information S5: Metabolic Concentrations for Simulation

The background of the 14 metabolites was typical for brain tumors, and identical in both cases: 4 mM glutamate, 7 mM glutamine, 1 mM γ-amino-butyric acid, 0.5 mM glutathione, 2 mM glycine, 8 mM Ins, 3 mM lactate, 5 mM NAA, 2 mM N-acetyl-aspartyl-

glutamate, 2 mM phosphocholine, 2 mM glycerol-phosphocholine, 3 mM Cr, 3 mM PCr, 2 mM taurine. T_2 relaxation times of 280 ms for NAA, 230 ms for phosphocholine and glycerol-phosphocholine, 150 ms for Cr and PCr, and 180 ms for all other metabolites including 2HG were considered (4).

Supporting Information S6: Comparing the Influence of Different Shimming Volumes for Metabolite Detection

For the comparisons of the influence of different shimming volumes, five shimming situations were measured in two healthy subjects (volunteers 3 and 4): 1) $2SH_{Box}$, 2) $2SH_{Brain}$ 3) $2SH_{Box}$+$ACDC_{metBox}$, 4) $2SH_{Box}$+$ACDC_{metBrain}$, 5) $2SH_{Brain}$+$ACDC_{metBrain}$. Due to time limitations, volunteer 3 could only be measured with the B0-mapping sequence, while volunteer 4 was also measured with the MRSI sequence. These measurements were performed to verify that AC/DC shimming provides additional improvements compared to the more optimized $2SH_{Brain}$ shimming over the brain region only, which is typically not available from manufacturers, but has been shown (23) to provide better performance for metabolite detection compared to $2SH_{Box}$. Because of the extended time (2 h) needed to acquire all five shim conditions, this comparison could be done only in two healthy subjects. For these measurements the fatScalp shim was not performed so that the difference in lipid suppression is not a confounding factor and covariate for the comparison of different shims during metabolite

detection. The ΔB_0, spectral linewidth, tCr/tNAA, tCr CRLB, and SNR maps as well as the ΔB_0-distribution and spectra were compared for all five different shim conditions.

Supporting Information Figure SF2 shows the measured B_0-maps, spectral linewidth maps, B_0-distribution and example spectra for these five different shim conditions in volunteer 4. The same measurements were performed in volunteer 3 and the corresponding mean standard deviations of volunteers 3-4 are printed on the B_0-maps in **Supporting Information Figure SF2**, demonstrating the improvements in global shim quality, which reduces the B_0 standard deviation by 15.7 % for $2SH_{Brain}$, 18.3 % for $2SH_{Box}$+$ACDC_{metBox}$, 33.9 % for $2SH_{Box}$+$ACDC_{metBrain}$, and 28.7 % for $2SH_{Brain}$+$ACDC_{metBrain}$ relative to $2SH_{Box}$. The improvement in local shim quality is additionally shown by the spectral linewidth maps obtained by LCModel fitting, with similar improvement in the mean linewidth. Both, the B_0-maps and the linewidth maps show strong improvements in the inferior slice which is the most challenging. The improvement in global shim quality is visible in the B_0-distribution plot showing narrower distributions when any of the $ACDC_{met}$ shims are superimposed on $2SH_{Box}$ or $2SH_{Brain}$. The improvement in local shim quality is shown by spectra from four voxels selected across the brain to span both AP and RL dimensions.

Supporting Information Figure SF3 shows the tCr/tNAA map, tCr CRLB and SNR map for the same five shim conditions and volunteer. These maps show that better shimming also translates to better quantification as demonstrated by a decrease in CRLB values and a corresponding increase in SNR.

Overall, these measurements show that the AC/DC hardware improves the 2SH shim regardless of shim volume. On the other hand, it is obvious that optimizing the 2SH shim or $ACDC_{met}$ over the brain volume is superior to shimming a box that includes also the scalp, since a smaller, more homogeneous volume can be shimmed better. The best results are obtained when shimming only the brain volume for both 2SH and AC/DC hardware.

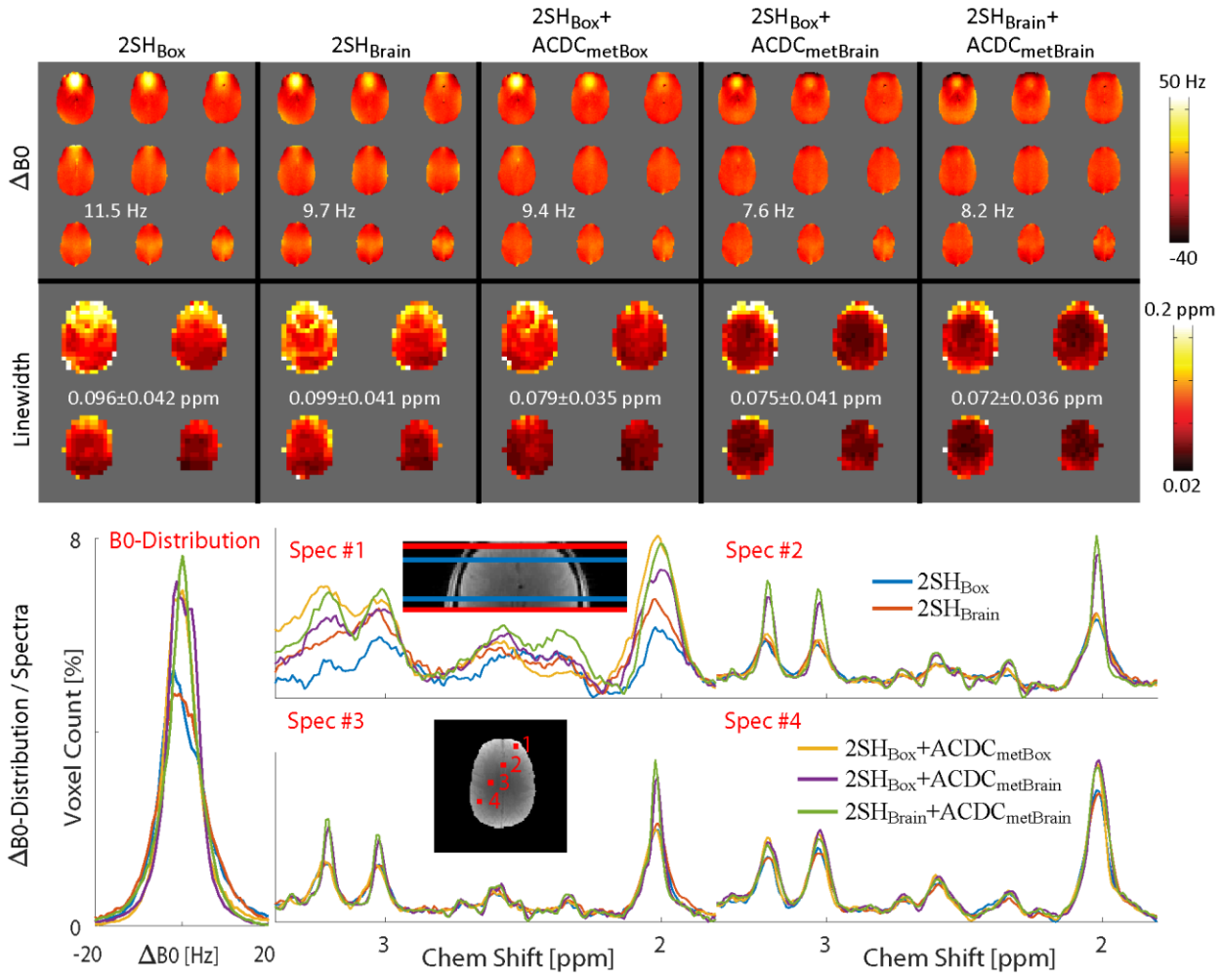

Supporting Information Figure SF2. B_0-maps, spectral linewidth maps, B_0-distribution plots, and spectra for five different shim conditions in a healthy volunteer: 1) 2SH optimized over the box shim volume ($2SH_{Box}$), 2) 2SH optimized over the brain ($2SH_{Brain}$), 3) $2SH_{Box}$ with the

$ACDC_{met}$ optimized over the box ($2SH_{Box}$+$ACDC_{metBox}$), 4) $2SH_{Box}$ with the $ACDC_{met}$ optimized over the brain ($2SH_{Box}$+$ACDC_{metBrain}$), and 5) 2SH and $ACDC_{met}$ optimized over the brain ($2SH_{Brain}$+$ACDC_{metBrain}$). The range of the B_0-slices (red), linewidth slices (blue). The standard deviation values printed over the B_0-maps (std over volunteer 3 and 4), and the mean and standard deviations of the linewidths over the linewidth maps (only volunteer 4). The spectra positions are indicated on the inlay anatomical images. The spectra and the B_0-distribution improve when using the ACDC hardware over $2SH_{Box}$ or $2SH_{Brain}$ alone.

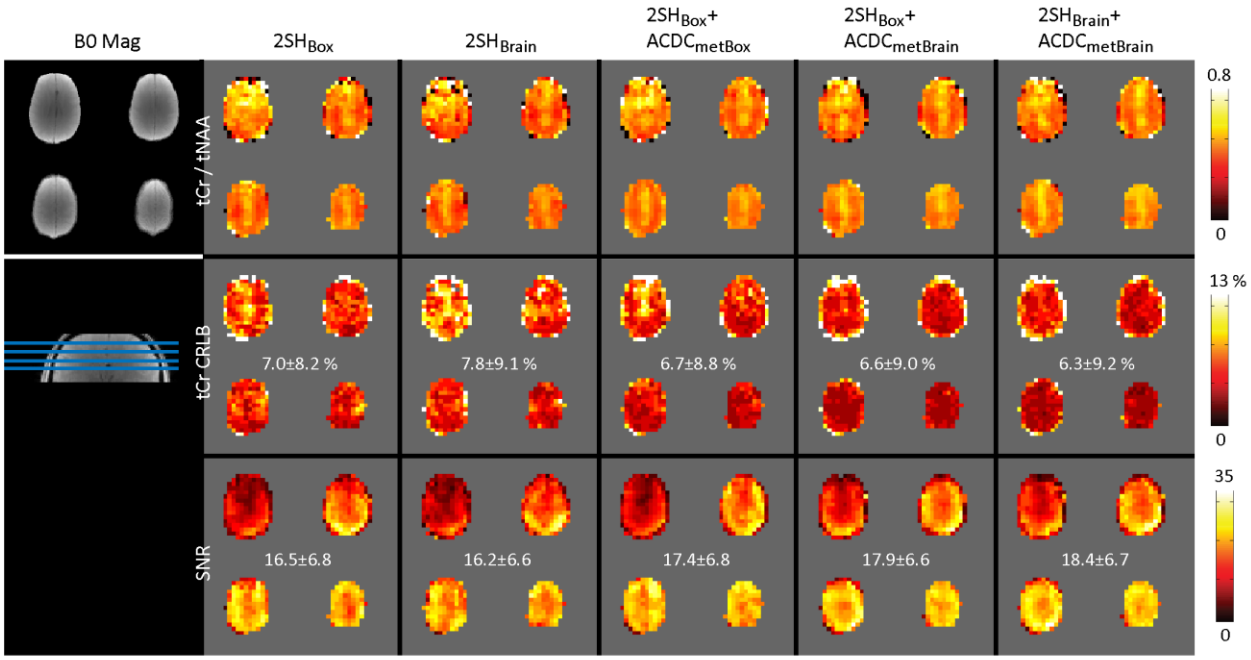

Supporting Information Figure SF3. tNAA/tCr maps, tCr CRLB maps, and SNR maps for the same volunteer and shim conditions as in **Supporting Information Figure S3**. The magnitude images show the position of the four MRSI slices. The tNAA/tCr map shows improved contrast between grey and white matter when using $2SH_{Box}$+$ACDC_{metBrain}$ in comparison to only using $2SH_{Box}$. The tCr CRLBs and SNRs show a clear improvement when using the AC/DC hardware in addition to 2SH for both box and brain shim volumes. The best results are obtained with $2SH_{Brain}$+$ACDC_{metBrain}$ when shimming the brain ROI for both 2SH and AC/DC.

Supporting Information S7: Reproducibility of AC/DC Hardware and Software

The reproducibility of the used methods was investigated in volunteer 5, which was measured three times with the B_0-mapping and MRSI sequence, and each time the subject and coil were repositioned in the scanner. Histograms, means, and standard deviations of the B_0-values were compared between the three repetitions.

Supporting Information Figure SF5 shows the repeatability results for the three shim conditions $2SH_{Box}$, $2SH_{Box}$+$ACDC_{metBrain}$ and $2SH_{Box}$+$ACDC_{fatScalp}$. The histograms of the B_0 values inside the brain shimmed volume have similar distribution for all three trials, with a half maximum width of 12.1±1.6 Hz for $2SH_{Box}$ and 6.7±0.6 Hz for $2SH_{Box}$+$ACDC_{metBrain}$, respectively. The corresponding spectral linewidths obtained from the MRSI data were 0.083±0.039 ppm, 0.081±0.040 ppm, 0.077±0.040 ppm for the three repetitions of $2SH_{Box}$, and 0.067±0.027 ppm, 0.063±0.024 ppm, 0.072±0.030 ppm for $2SH_{Box}$+$ACDC_{metBrain|fatScalp}$. The SNR's were 14.8±6.7, 15.8±6.6, 16.1±6.4 for $2SH_{Box}$, and 16.7±6.9, 16.2±6.6, 16.7±6.5 for $2SH_{Box}$+$ACDC_{metBrain}$. The B_0 histograms for fat suppression with $2SH_{Box}$+$ACDC_{fatScalp}$ showed 151.3±0.6 Hz for the frequency separation between the fat peak at 1.25 ppm and the NAA peak at 2 ppm, which is an increase by 50 Hz compared to $2SH_{Box}$ alone.

These results showed good inter-scan reproducibility of all three types of shimming methods, $2SH_{Box}$, $2SH_{Box}$+$ACDC_{metBrain}$ and $2SH_{Box}$+$ACDC_{fatScalp}$, with only small variations. The variation in $2SH_{box}$+$ACDC_{metBrain}$ shimming is slightly smaller (CV = 10%) than the variation in the $2SH_{box}$ baseline shimming (CV = 13%), indicating that $ACDC_{metBrain}$ shimming is highly reproducible and effective in reducing the variability of $2SH_{box}$ baseline shimming, and demonstrates that the AC/DC hardware and software perform reliably.

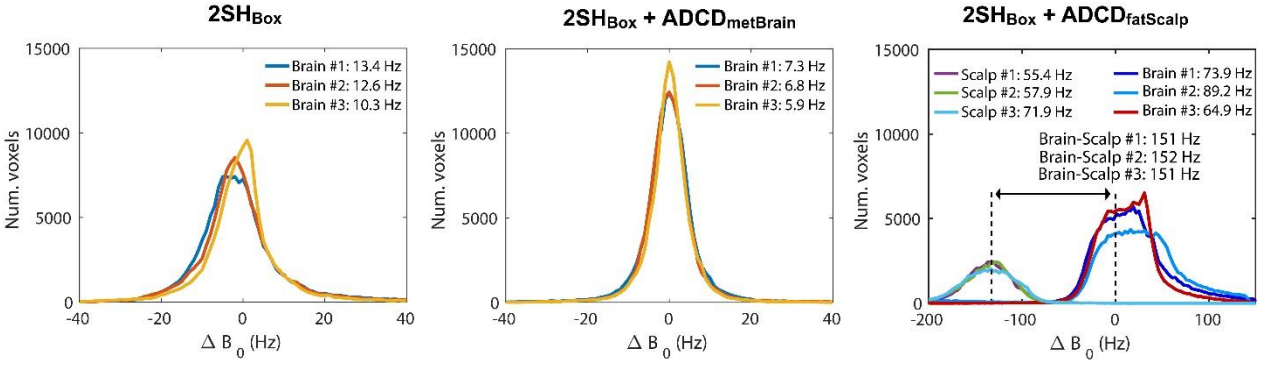

Supporting Information Figure SF5. Repeatability results for the three shim conditions: 1) $2SH_{Box}$, 2) $2SH_{Box}$+$ACDC_{metBrain}$, and 3) $2SH_{Box}$+$ACDC_{fatScalp}$. Overlay of the B_0 histograms from the corresponding shimmed volumes of every trial are shown for each shim condition. The histograms of the B_0 values used for metabolite detection have a similar distribution for all three trials, with a half maximum width of 12.1±1.6 Hz for $2SH_{Box}$, and 6.7±0.6 Hz for $2SH_{Box}$+$ACDC_{metBrain}$, respectively. The corresponding spectral linewidths obtained from the MRSI data were 0.083±0.039 ppm, 0.081±0.040 ppm, 0.077±0.040 ppm for the three repetitions of $2SH_{Box}$, and 0.067±0.027 ppm, 0.063±0.024 ppm, 0.072±0.030 ppm for $2SH_{Box}$+$ACDC_{metBrain|fatScalp}$. The SNR's for the same conditions were 14.8±6.7, 15.8±6.6, 16.1±6.4, and 16.7±6.9, 16.2±6.6, 16.7±6.5. The B_0 histograms for fat suppression with the $2SH_{Box}$+$ACDC_{fatScalp}$ shim had half maximum width of 76±12.3 Hz in the scalp ring volume, 61.7±8.9 Hz in the brain volume, and 151.3±0.6 Hz for the separation between the fat signal at 1.2 ppm and the NAA signal at 2 ppm. By comparison, in the case of $2SH_{Box}$ the half maximum width was 32.7±3.2 Hz in the scalp ring volume, 12.1±1.6 Hz in the brain volume, and 101.9±0.9 Hz for the separation between the fat signal at 1.25 ppm and the NAA signal at

2 ppm. The $ACDC_{fatScalp}$ increased the separation between fat and NAA by 50 Hz, which is significant considering that the HGSB pulse has a transition band of 48 Hz.

Supporting Information S8: Sample Spectra in Healthy and Tumor Tissue of Patient 1

Supporting Information Figure SF6 shows sample spectra together with the 2HG fit from the healthy and tumor tissue of patient 1 for $2SH_{Box}$ and $2SH_{Box}+ACDC_{metBrain|fatScalp}$.

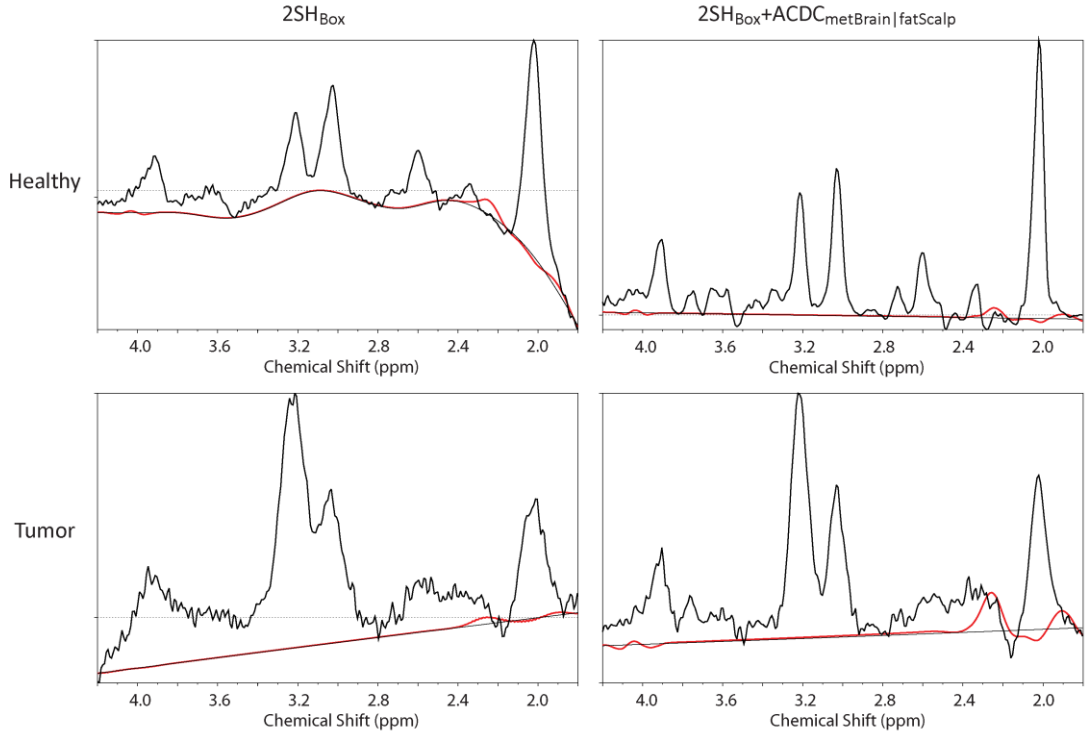

Supporting Information Figure SF6. Sample spectra with LCModel fits of the 2HG contribution (red curve) from voxels shown by red arrows in patient 1 (Fig. 5), containing healthy tissue and tumor tissue for the $2SH_{Box}$ and $2SH_{Box}+ACDC_{metBrain|fatScalp}$ shims, respectively. Narrower linewidths due to more uniform B0 field in the brain and flatter baselines due to better lipid/water suppression provide better 2HG fits in $2SH_{Box}+ACDC_{metBrain|fatScalp}$ spectra. The intensity of spectra is given in arbitrary units.

Supporting Information S9: Comparison of 2HG Maps in Native and Interpolated Resolution

Supporting Information Figure SF7 shows the comparison of the interpolated and native resolution for Patient 1, 3, and 4, while Supporting Information Figure SF8 shows the same for Patient 2, Volunteer 1, and Volunteer 2. The 2HG foci in the tumor region, e.g. of patient 1 are visible in both cases, but the pixelation artifact cannot be seen in the interpolated maps.

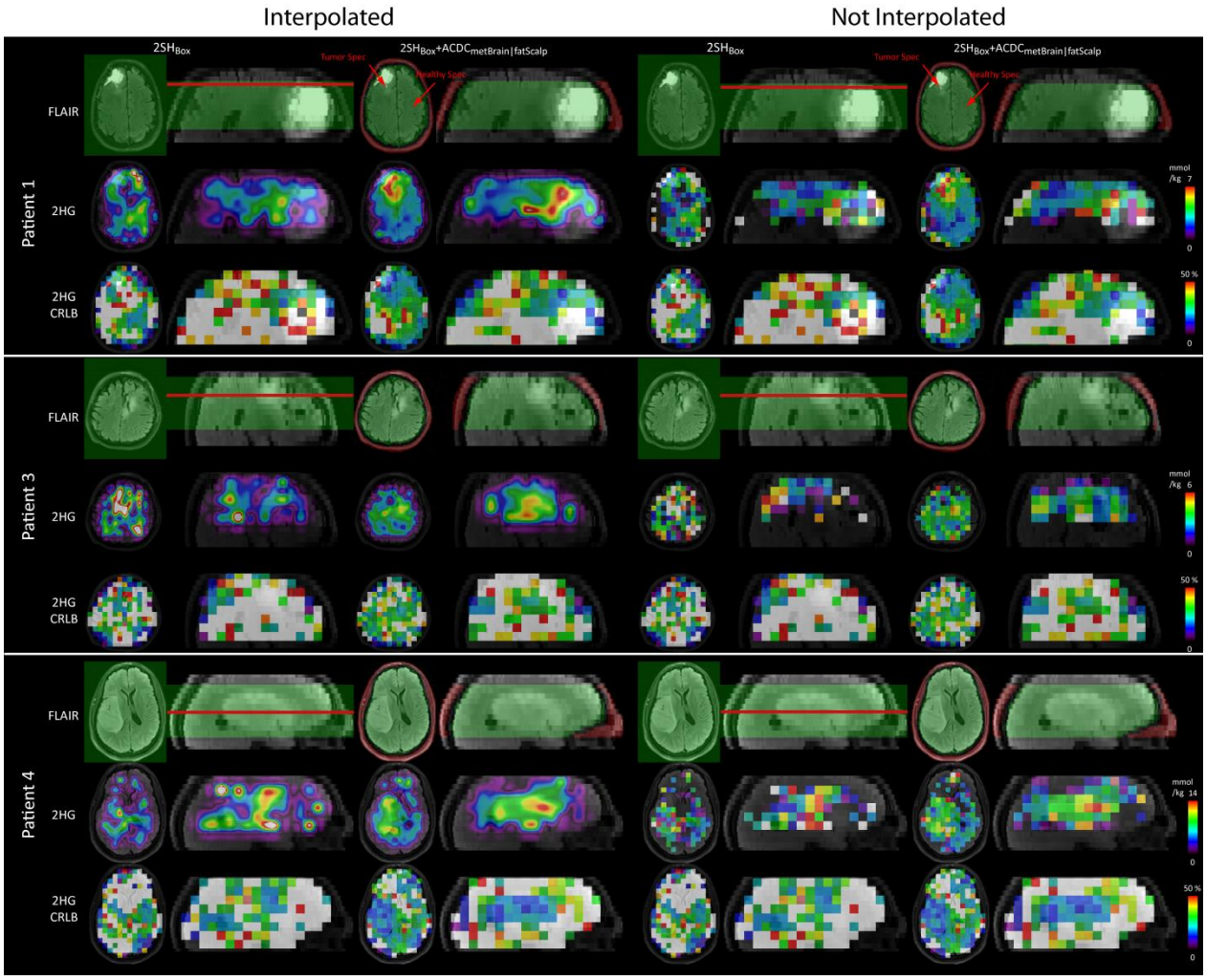

Supporting Information Figure SF7: Comparison of interpolated and native resolution of the 2HG maps of Patient 1, 3 and 4. The interpolated maps are the same as Figure 5.

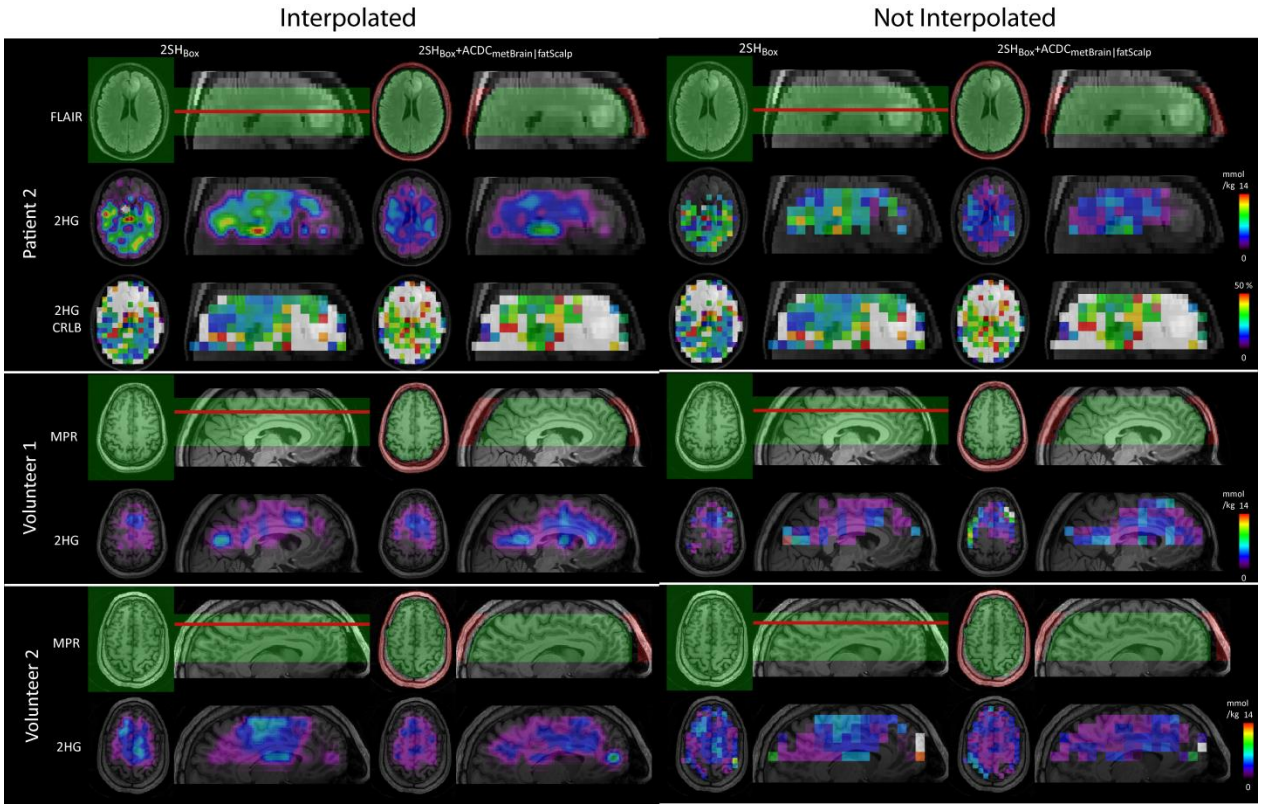

Supporting Information Figure SF8: Comparison of interpolated and native resolution of the 2HG maps of Patient 2, Volunteer 1, and 2. The interpolated maps are the same as Figure 6.